PERGAMON

International Journal of Solids and Structures 36 (1999) 3755–3777

INTERNATIONAL JOURNAL OF SOLIDS and STRUCTURES

A nonlinear viscoelastic constitutive model of solid propellant

Gyoo-Dong Jung*[,1], Sung-Kie Youn

Department of Mechanical Engineering, Korea Advanced Institute of Science and Technology, 373-1, Kusung, Yusung, Taejon, 305-701, Korea

Received 29 September 1997; in revised form 29 May 1998

Abstract

A nonlinear viscoelastic constitutive model for solid propellant is proposed. The viscoelastic dewetting criteria is developed and the softening of the solid propellant due to damage is treated by the modulus decrease. In the calculation of the modulus decrease, the modulus of void, which is created by dewetting, is modeled with non zero constant values. The values of adhesion energy between the binder and AP particle are obtained by a modified 180° peel test. The nonlinearities during cyclic loading are accounted for by the functions of the octahedral shear strain measure. The model is evaluated with different loading conditions and the predicted values well matched the measured ones. The model provides a simple and convenient means to predict solid propellant behavior without requiring a complex micromechanical description.
© 1999 Elsevier Science Ltd. All rights reserved.

1. Introduction

Composite solid propellants are considered as lightly cross-linked, long chain polymers filled with solid particles. These materials exhibit highly nonlinear viscoelastic response due to the damage process such as Mullin's effect, debonding, vacuole formation and cracking under various loading history. A number of studies have been performed to address one or more of these factors contributing to the nonlinear behavior of the solid propellants (Farris and Schapery, 1973; Swanson and Christensen, 1983; Shapery, 1986; Simo, 1987; Vratanos and Farris, 1993; Ravichandran and Liu, 1995; Özüpek and Becker, 1996). However, practically useful constitutive frameworks for solid propellant behavior are not readily available. It is hard to determine the parameters required in the various models for accurate predictions of the propellant behavior.

It has been known that the main sources of solid propellant nonlinearities are the Mullin's effect

* Corresponding author. Fax: 0082 042 821 2224; E-mail: vejung@sunam.kreonet.re.kr

[1] Present address: 4-4-1, Yusung, P.O. Box 35-4, Taejon, 305–600 South Korea.

0020–7683/99/$ - see front matter © 1999 Elsevier Science Ltd. All rights reserved
PII: S0020–7683(98)00175–9

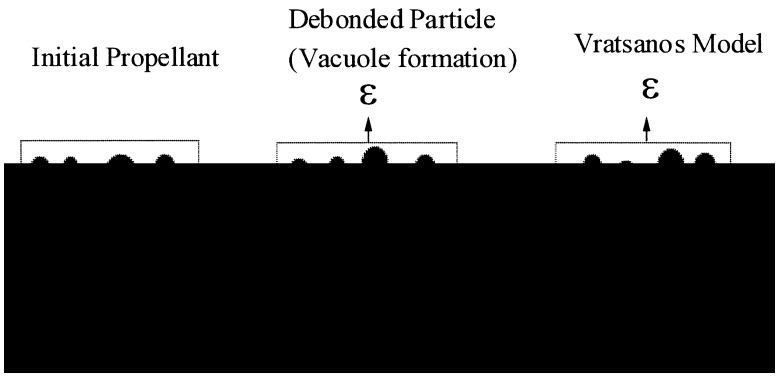

Fig. 1. Debonding model used in the Vratsanos–Farris model.

and dewetting (Farris and Schapery, 1973). Mullin's effect is caused by the highly non-uniform stress and strain gradient in the polymer matrix at small strains. At large strains, after sufficient microstructural damage has occurred, debonding begins in the polymer–filler interface and vacuoles form. These dewetting phenomenon naturally occurs in the zone of maximum damage which would depend on the local polymeric composition, bond strength, local packing characteristics, local distribution of chain length and many other unknown factors. These microscopic changes make the solid propellant lose its initial stiffness and change its bulk character from incompressible to compressible behavior. Under these influences, solid propellants exhibit very complicated behavior including the features associated with time–temperature effects.

A representative dewetting mode when subjected to loading is shown in Fig. 1 (Vratsanos and Farris, 1993). Under straining, damage occurs either by debonding and/or vacuole formation. Upon loading, at a critical strain or stress level, the particles separate from the matrix causing dewetting. This introduces volume dilatation and results in nonlinearity in the stress–strain behavior. The stress–strain response is nearly linear viscoelastic when there is little or no volume dilatation and the nonlinearity sets in once the dilatation becomes significant. The uniaxial response and the accompanying volume dilatation of solid propellants have been investigated by a number of researchers (Farris and Schapery, 1973; Vratanos and Farris, 1993; Özüpek and Becker, 1996). From these studies, it has been observed that the stress–strain response of solid propellants undergoing damage can be related to the constitutive response of the undamaged propellants and the corresponding volume dilatation (Vratanos and Farris, 1993; Ravichandran and Liu, 1995; Özüpek and Becker, 1996). Of greater interest is a technique that would permit the prediction of overall stress–strain behavior. Recently, Vratsanos and Farris (1993) developed such a model based on the classical linear elastic theory and the first law of thermodynamics. This model is simple, but its elastic behavior is not suitable for predicting the viscoelastic behavior that is significant in solid propellant.

In the present study, a simple, nonlinear viscoelastic constitutive model of composite solid propellant is proposed. In the model, the damage is accounted for by the modulus decrease due to dewetting.

2. The constitutive model

In order to develop the damage model, the changes that occur during the dewetting process must be mathematically described. The dewetting model is based on the elastic dewetting criteria developed by Vratsanos and Farris (1993).

2.1. The Vratsanos–Farris dewetting criteria

The Vratsanos–Farris model (1993) is based on the energy principle that work energy input in the material must be either stored as internal strain energy or be used to create new surface area through the process of debonding between particles and matrix or be some combination of the two. This model is based on the assumptions that both the propellant and matrix are linearly elastic and the debonding process only is the cause of the nonlinear stress–strain behavior.

The energy balance in the debonding process can be written through a modified first law of thermodynamics as follows:

$$\delta U_{\text{strain}} + \delta U_{\text{surface}} = \delta W + \delta Q \tag{1}$$

where δU_{strain} is the net strain energy in system, $\delta U_{\text{surface}}$ the net surface energy dissipated, δQ the net heat transferred into system, and δW the net external work done on system. By using the virtual work principle under adiabatic conditions, the surface energy released can be shown to be related to the variations in the stress and strain by

$$2G_{\text{c}}\frac{\delta A}{V_{\text{o}}} = \sigma_{ij}\delta\varepsilon_{ij} - \delta\sigma_{ij}\varepsilon_{ij} \tag{2}$$

where G_{c} is the adhesion energy between the matrix and the filler, V_{o} the unit volume, and A the debonded surface area. The above equation can be solved for the critical strain at which the particle will debond. Vratsanos derived an equation applicable for a uniaxial tensile test by using eqn (2) along with linear elastic constitutive equations.

The final equation for a uniaxial tensile bar under atmospheric pressure was given as:

$$-2\frac{G_{\text{c}}}{V_{\text{o}}}\frac{\text{d}A}{\text{d}c} = \varepsilon_{11}^2\frac{\text{d}E}{\text{d}c} \tag{3}$$

where c is the current filler concentration, ε_{11} the uniaxial strain, and E the propellant modulus.

When the particles are spherical in shape, the change in surface area with respect to the change in volume fraction in terms of particle radius R was obtained as eqn (4) by accounting the fact that two surfaces were created when a particle was debonded, one in the matrix and the other on the filler.

$$\frac{\text{d}A}{\text{d}c} = -6V_{\text{o}}/R \tag{4}$$

The dewetting causes loss of reinforcement in the propellant. Modulus changes based on filler volume fraction were calculated using the Farber–Farris equations (Farber and Farris, 1987):

$$\frac{\mathrm{d}G}{\mathrm{d}c} = \frac{-15G(1+v)\left(1-\dfrac{G_i}{G}\right)}{\left\{7-5v+2(4-5v)\dfrac{G_i}{G}\right\}(1-c)}$$

$$\frac{\mathrm{d}K}{\mathrm{d}c} = \frac{K-K_i}{\left\{1+\dfrac{K_i-K}{K+3/4G}\right\}(1-c)} \tag{5}$$

where G is the shear modulus of propellant, v Poisson's ratio of propellant, K the bulk modulus of propellant, and K_i, G_i the moduli of filler.

In Vratsanos–Farris model, the debonded particles were eliminated from the composites and replaced with voids of equal sizes. All particles were eventually replaced by voids.

Using eqns (3)–(5), the critical strain at which a particle of a particular diameter would debond could be calculated knowing the state of adhesion and the mechanical properties of the constituent materials.

2.2. Proposed viscoelastic dewetting criteria

In order to predict the stress–strain behavior of solid propellants, viscoelastic effect should be considered. The assumptions made in the formulation of the viscoelastic damage model are:

(1) The composite propellant and matrix are linearly viscoelastic.
(2) The debonding process only is the cause of the nonlinear stress–strain behavior of the propellant.
(3) The overall material is homogeneous and isotropic.
(4) The time characteristics of the propellant behavior are not changed by the debonding process.

The first assumption is valid at the low strain before the initiation of debonding. The second and third assumptions are the same as in the Vratsanos–Farris model. The validity of the last assumption will be discussed later.

The linear viscoelastic constitutive relation for thermorheologically simple material can be written as by representing the relaxation modulus E_{rel} with the prony series.

$$\begin{aligned}\boldsymbol{\sigma}(t) &= \int_0^t E_{\mathrm{rel}}(t-\tau)\dot{\boldsymbol{\varepsilon}}(\tau)\,\mathrm{d}\tau \\ &= \int_0^t \left(E_\infty + \sum_i^n E_i e^{-(t-\tau)/\tau_i}\right)\dot{\boldsymbol{\varepsilon}}(\tau)\,\mathrm{d}\tau\end{aligned} \tag{6}$$

where E_∞ represent the long term modulus.

This equation can be rewritten in the form (ABAQUS, 1995)

$$\boldsymbol{\sigma}(t) = E_{\mathrm{o}}\left(\boldsymbol{\varepsilon} - \sum_{i=1}^{n} \alpha_i \boldsymbol{\varepsilon}_{\mathrm{Vi}}\right) \tag{7}$$

where E_{o} is the glassy modulus, $\alpha_i = E_i/E_{\mathrm{o}}$ is the relative modulus of term i and

$$\boldsymbol{\varepsilon}_{\mathrm{Vi}} = \int_0^t [1 - e^{-(t-\tau)/\tau i}\dot{\boldsymbol{\varepsilon}}(\tau)]\,\mathrm{d}\tau \tag{8}$$

is the viscous strain in each term of the series.

The energy dissipation for the infinitesimal strain increment, $\Delta U_{\mathrm{dissipation}}$ is

$$\begin{aligned}\Delta U_{\mathrm{dissipation}} &= \tfrac{1}{2}(\boldsymbol{\sigma}_{n+1} + \boldsymbol{\sigma}_n) : \sum_i^n \alpha_i \Delta\boldsymbol{\varepsilon}_{\mathrm{Vi}} \\ &= \tfrac{1}{2}(\boldsymbol{\sigma}_{n+1} + \boldsymbol{\sigma}_n) : \left[\Delta\boldsymbol{\varepsilon} - \frac{1}{E_{\mathrm{o}}}(\boldsymbol{\sigma}_{n+1} - \boldsymbol{\sigma}_n)\right] \\ &= \Delta W - \Delta U_{\mathrm{strain}}\end{aligned} \tag{9}$$

where the total work, W and the elastic energy increase U_{strain} are respectively

$$\Delta W = \tfrac{1}{2}(\boldsymbol{\sigma}_{n+1} + \boldsymbol{\sigma}_n) : \Delta\boldsymbol{\varepsilon} \tag{10}$$

$$\Delta U_{\mathrm{strain}} = \frac{1}{2E_{\mathrm{o}}}(\boldsymbol{\sigma}_{n+1} : \boldsymbol{\sigma}_{n+1} - \boldsymbol{\sigma}_n : \boldsymbol{\sigma}_n) \tag{11}$$

So, the elastic energy of viscoelastic solid is

$$U_{\mathrm{strain}} = \frac{1}{2E_{\mathrm{o}}}(\boldsymbol{\sigma} : \boldsymbol{\sigma}) \tag{12}$$

The strain energy can be decomposed into the deviatoric and volumetric stresses, S'_{ij}, σ_{ii}

$$U_{\mathrm{strain}} = \frac{1}{4G_{\mathrm{o}}} S'_{ij} S'_{ij} + \frac{1}{18K_{\mathrm{o}}} \sigma_{ii}\sigma_{kk} \tag{13}$$

The net strain energy is then

$$\delta U_{\mathrm{strain}} = \delta\left(\frac{1}{4G_{\mathrm{o}}}\right) S'_{ij} S'_{ij} + \frac{1}{4G_{\mathrm{o}}}\delta(S'_{ij} S'_{ij}) + \delta\left(\frac{1}{18K_{\mathrm{o}}}\right)\sigma_{ii}\sigma_{kk} + \frac{1}{18K_{\mathrm{o}}}\delta(\sigma_{ii}\sigma_{kk}) \tag{14}$$

where G_{o} and K_{o} represent the glassy shear and bulk modulus, respectively. Also, the net work δW is

$$\begin{aligned}\delta W &= \sigma_{ii}\delta\varepsilon_{ij} \\ &= S'_{ij}\delta e_{ij} + \frac{\sigma_{ij}}{3}\delta e\end{aligned}$$

$$= S'_{ij}\delta\left[\frac{S'_{ij}}{2G_o} + \sum_{k=1}^{n}\frac{G_k}{G_0}(e_{ij})_{Vk}\right] + \frac{\sigma_{ii}}{3}\delta\left[\frac{\sigma_{kk}}{3K_o} + \sum_{k=1}^{n}\frac{K_k}{K_0}(e)_{Vk}\right]$$

$$= S'_{ij}\delta\left(\frac{S'_{ij}}{2G_o}\right) + \frac{\sigma_{ii}}{3}\delta\left(\frac{\sigma_{kk}}{3K_o}\right) + \delta W_V \tag{15}$$

where G_k, K_k are the prony series constant of shear and bulk relaxation modulus respectively, $(e_{ij})_{Vk}$, $(e)_{Vk}$ are the viscous deviatoric strain and viscous dilatation in each term k of the prony series, and W_V is the work dissipated.

The energy balance equation, eqn (1) for the viscoelastic solid can be written as follows:

$$\delta U_{strain} + \delta U_{surface} + \delta U_{dissipation} = \delta W + \delta Q \tag{16}$$

The initial surface energy $\delta U_{surface}$ is the energy consumed to create new dewetted surfaces and is proportional to the surface area exposed in each debonding process. Therefore, the surface energy can be represented using a proportionality constant, G_c that is simply the adhesion energy.

$$\delta U_{surface} = G_c \delta A / V_o \tag{17}$$

Also, $\delta W_V = \delta U_{dissipation}$, and $\delta Q = 0$ for the adiabatic process.

By using the chain rule, all the differential quantities can be put on a volume fraction basis. Equation (16), can then be solved for the critical stress at which the first particle will debond

$$\frac{6}{R}G_c = \frac{S'_{ij}S'_{ij}}{4G_o^2}\frac{dG_o}{dc} + \frac{\sigma_{ii}\sigma_{kk}}{18K_o^2}\frac{dK_o}{dc} \tag{18}$$

Equation (18) is the viscoelastic dewetting criteria of solid propellant and can be solved for the critical stress at which the particle will debond. The change of moduli with dewetting can be calculated by eqn (5).

2.3. Viscoelastic constitutive equation

The large strain capability of solid propellant requires that the stress–strain relation be formulated in terms of the appropriate stress and strain tensors. This is most easily handled by means of Lagrangian description of the material deformation using the second Piola–Kirchhoff stress and Green strain tensors. For this, Simo's model for stress–strain behavior is adopted and modified in this study.

Simo's model (1987) is mainly characterized by the uncoupled bulk and deviatoric responses over any range of deformations. The proper decomposition in the nonlinear range is accomplished by the kinematic split of the deformation gradient F into volume-preserving and deviator components as

$$\boldsymbol{F} = J^{1/3}\bar{\boldsymbol{F}} \tag{19}$$

where J is the det $\boldsymbol{F}$ and $\bar{\boldsymbol{F}}$ is the volume preserving part of $\boldsymbol{F}$.

This model is based on the definition of an uncoupled free energy function Ψ of the form

$$\Psi(\boldsymbol{E}, \boldsymbol{Q}) = U^o(J) + \bar{\Psi}^o(\bar{\boldsymbol{E}}) - \boldsymbol{Q} : \bar{\boldsymbol{E}} + \Psi_I(\boldsymbol{Q}) \tag{20}$$

where U^o and $\bar{\Psi}^o$ are the uncoupled volumetric and deviatoric parts of the initial elastic stored energy, $\boldsymbol{Q}$ is an internal variable, Ψ_I is a function to be determined from the conditions of thermodynamic equilibrium and $\bar{\boldsymbol{E}}$ is the volume preserving part of Green strain $\boldsymbol{E}$. For the isothermal case, the second Piola–Kirchhoff stress tensor $\boldsymbol{S}$ is obtained from

$$\boldsymbol{S} = \frac{\partial \psi(\boldsymbol{E}, \boldsymbol{Q})}{\partial \boldsymbol{E}} \tag{21}$$

The viscoelastic behavior is introduced through the evolution equation of the internal variable $\boldsymbol{Q}$.

In this study, Simo's constitutive relation is modified by considering the viscoelastic bulk response and introducing the volumetric and deviatoric damage functions, D_{V}, D_{d}. The resulting constitutive equation is of the following form

$$\boldsymbol{S}(t) = D_{\mathrm{V}} \times J\boldsymbol{C}^{-1}\left\{\int_0^t \frac{K[\xi(t)-\xi(\tau)]}{K_{\mathrm{o}}}\frac{\partial}{\partial\tau}\left[\frac{\partial U^o}{\partial J}\right]\mathrm{d}\tau\right\} + D_{\mathrm{d}} \times J^{-2/3}\,\mathrm{DEV}\left\{\int_0^t \frac{G[\xi(t)-\xi(\tau)]}{G_{\mathrm{o}}}\frac{\partial}{\partial\tau}\mathrm{DEV}\left[\frac{\partial \bar{\psi}^o}{\partial \bar{\boldsymbol{E}}}\right]\mathrm{d}\tau\right\} \tag{22}$$

where $\boldsymbol{C}$ is the right Cauchy–Green deformation tensor,

$$\mathrm{DEV}(\bullet) = (\bullet) - 1/3(\bullet : \boldsymbol{C})\boldsymbol{C}^{-1}, \tag{23}$$

$$\xi(t) = \int_0^t \frac{\mathrm{d}\eta}{a_{\mathrm{T}}[T(\eta)]}, \xi(\tau) = \int_0^\tau \frac{\mathrm{d}\eta}{a_{\mathrm{T}}[T(\eta)]}, \tag{24}$$

T is temperature, and a_{T} is time–temperature shift factor.

Equation (22) accounts for the large deformation through a suitable definition of energy. The Neo–Hookean hyperelastic energy model is used to represent the deviatoric strain energy of the solid propellant.

$$U^o(J) = \frac{K}{2}(J-1)^2$$

$$\bar{\Psi}^o(\bar{\boldsymbol{E}}) = C_1(\bar{I}_1 - 3) \tag{25}$$

where $\bar{I}_1$ is the first strain invariant of $\bar{\boldsymbol{C}}$.

The Neo–Hookean coefficient C_1 can be calculated from the uniaxial stress–strain relation under incompressibility assumption before dewetting and the result is

$$C_1 = \tfrac{1}{2}G_{\mathrm{o}} \tag{26}$$

For the comparison with the measured stress, the engineering reference stress T_{ij} can be calculated by

$$T_{ij} = F_{ik}S_{kj} \tag{27}$$

In this model, strain softening by dewetting can be accounted for through the modulus decrease which is determined by the viscoelastic dewetting criteria, eqns (18) and (5). Also, in order to

include the cyclic effects, i.e. the rapid decrease of stress during the unloading and hysteresis in cyclic loading, the function f is introduced, which was introduced by Özüpek and Becker (1996). So, the damage functions D_v, D_d can be expressed as

$$D_v = \frac{K_D}{K} \times f \tag{28}$$

$$D_d = \frac{G_D}{G} \times f \tag{29}$$

where K_D, G_D are the decreased propellant moduli due to dewetting,

$$f = f_u\left(\frac{\bar{I}_\gamma}{\bar{I}_{\gamma max}}\right) \quad \text{at unloading from a loading curve}$$

$$f = f_u\left(\frac{\bar{I}_\gamma}{\bar{I}_{\gamma max}}\right) \times f_{r/u}(\bar{I}_{rel}) \quad \text{at reloading or unloading from a reloading curve} \tag{30}$$

and $f_{r/u}$ is the ratio of f_r and f_u. The strain measure $\bar{I}_\gamma$ is incorporated to represent the effect of distortion and this can be expressed in terms of volume preserving octahedral shear strain measure (Özüpek and Becker, 1996)

$$\bar{I}_\gamma = \tfrac{1}{6}(2\bar{I}_1^2 - 6\bar{I}_2)^{1/2} \tag{31}$$

$\bar{I}_{\gamma max}$ represents the maximum $\bar{I}_\gamma$ previously achieved during the loading history.

Also, $\bar{I}_{rel}$ is used to keep the continuity in the stress response on reversing the loading direction, which is defined as (Özüpek and Becker, 1996)

$$\bar{I}_{rel} = \frac{\bar{I}_\gamma - \bar{I}_{\gamma min}}{\bar{I}_{\gamma max} - \bar{I}_{\gamma min}} \tag{32}$$

where $\bar{I}_{\gamma min}$ is the value at the end of unloading.

The algorithm for the implementation of the model in a computer program to predict stress–strain behavior can be summarized as follows:

Initial propellant properties and configuration:

(1) Specify mechanical properties of the solid propellant, matrix, filler, void and adhesion energy.
(2) Specify initial statistical distribution of filler particle size.

Deformation of solid propellant:

(3) Calculate the viscoelastic stress by eqn (22).
(4) Check, with eqn (18), whether dewetting occurs at this stress for the largest particles.
(5) If dewetting occurs, reduce the dewetted filler volume fraction and increase the void volume fraction by the same amount.
(6) Calculate the reduced relaxation modulus and damage functions by eqn (5, 28, 29).
(7) Calculate the reduced nonlinear viscoelastic stress by eqn (22).
(8) Calculate the next dewetting stress for the particles that are not dewetted.

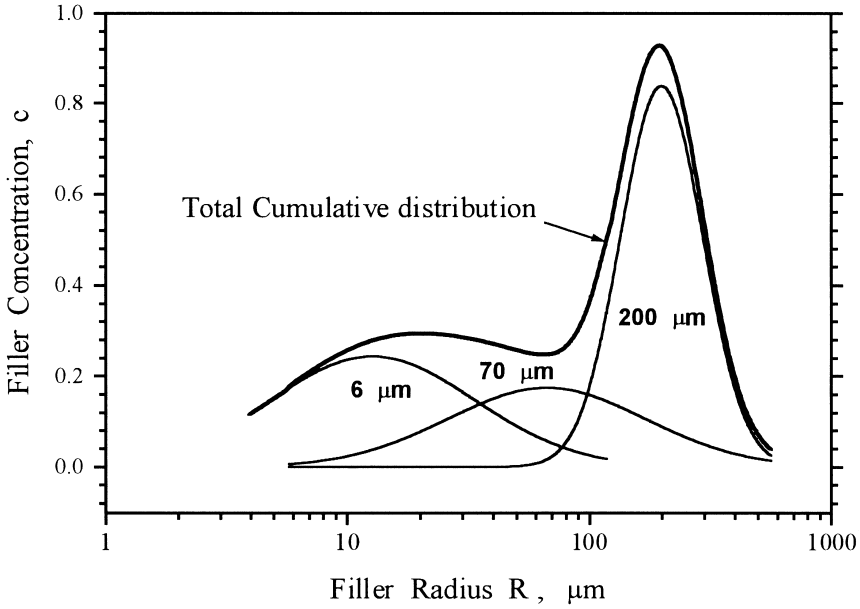

Fig. 2. Filler size distribution for the solid propellant used.

Repeat calculations from step 4 to 8 until there is no particle remaining.

3. Experiment

The experimental work in this study consists of three major objectives. The first is to characterize the linear/nonlinear relaxation modulus of the solid propellant to verify the damage characteristics. The second is the relaxation test to confirm the applicability of the Farber–Farris eqn (5). The last is the constant rate test and complex loading test to verify the validity of the present viscoelastic model. In the constant rate test, volume dilatations were measured by gas dilatometer. The material used in this work is an HTPB solid propellant with 76% particle volume fraction of AP (ammonium perchlorate) and Al (aluminum) powder. The propellant has some additives to enhance ballistic and mechanical properties and also has bonding agents to improve the adhesion. Each set of particles was sized using a Malvern Series particle sizer and size distribution plus the cumulative distribution are plotted in Fig. 2. The average diameters of AP particles are 6, 70 and 200 μm. As a result of the visual inspections using the microscope, the shape of AP particles is found out to be ellipsoidal in general and that of Al is spherical. Uniaxial, simple shear and pocker chip tests are used. The uniaxial specimen chosen is wooden tab end bar type and its gage length is the wood-to-wood distance. Its effective gage length does not change with strain (Kugler et al., 1990). The specimens are shown in Fig. 3. The specimen surface is mill machined and bonded to wood and Al tab with the polyurethane adhesive. Four specimens are tested at each test condition and stress responses are averaged. All tests are performed in an Instron 1122 in the humidity controlled room

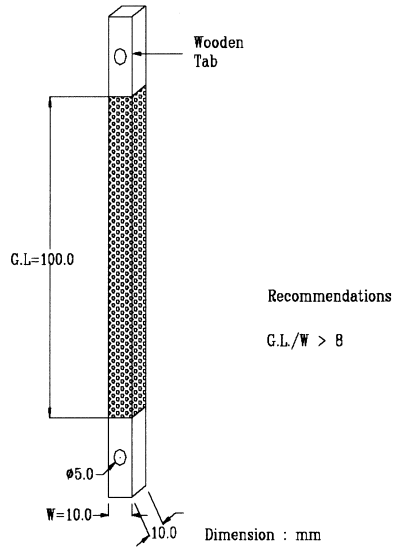

A. Uniaxial wooden tab end specimen

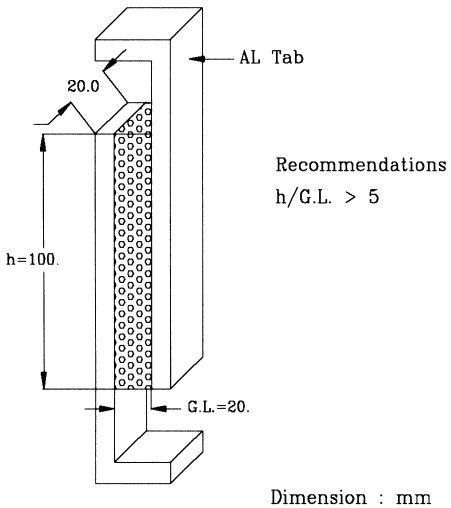

B. Simple shear specimen

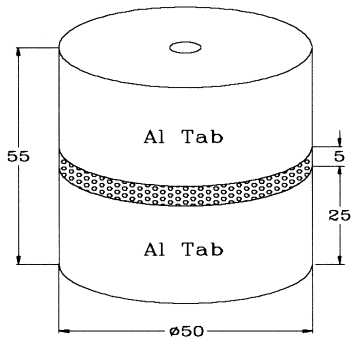

C. Pocker chip specimen

Fig. 3. Specimen geometries and dimensions.

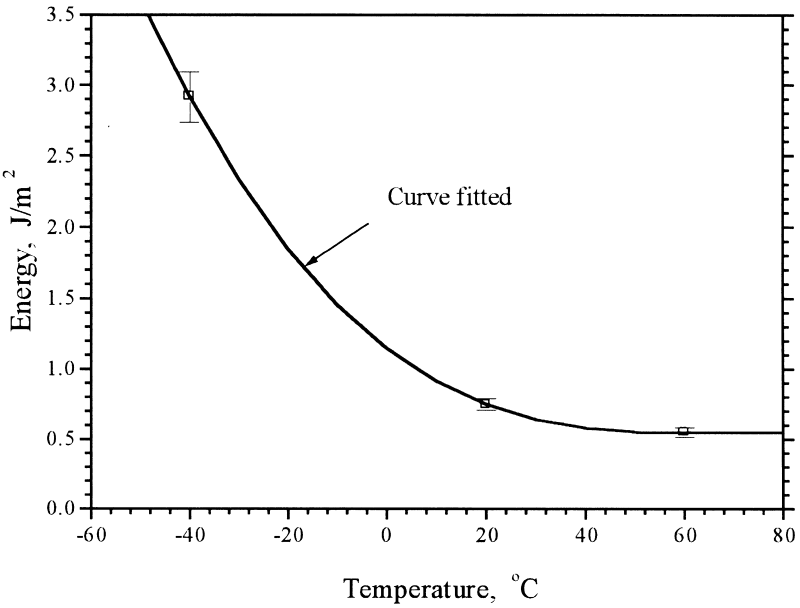

Fig. 4. Adhesion energies between binder and AP.

(RH $< 30\%$). Prior to testing, the specimens are conditioned at each test temperature for more than 1 h.

The values of adhesion energy are investigated by using a modified ASTM 180° peel test on the binder material bonded to AP plate, which is one inch wide and five inches long (ASTM Standard, no. D903-93). AP plate is made by pressing the fine AP particles in a mold with high pressure of 3000 kg cm^{-2}. After molding, the surface of AP plates is treated by methyl alcohol for recrystallization. The surface treatment is used to fill up any micro gap in the surface. The unfilled binder is cast onto the AP plates and an inextensible backing of cotton textile is lightly placed onto the binder. The backing cloth is necessary to achieve a constant rate of separation between the binder and AP filler since the binder exhibits large extension. The rate of separation is 100 mm min^{-1}. Five specimens at each temperature of 60, 20 and -40°C are tested and the peeling forces are averaged. The peeling forces are converted to the energies and the adhesion energies thus obtained are plotted in Fig. 4.

4. Results and discussion

4.1. The stress relaxation test of the solid propellant

The linear (small strain) uniaxial and shear stress relaxation tests are carried out respectively at stretch ratio $\lambda = 1.02$, and shear strain $\varepsilon_{12} = 2.5\%$ in the temperature range of $-90 \sim 60$°C with the strain rate 50% min^{-1}. In the shear relaxation test, $\varepsilon_{12} = 2.5\%$ is applied, so the specimen is

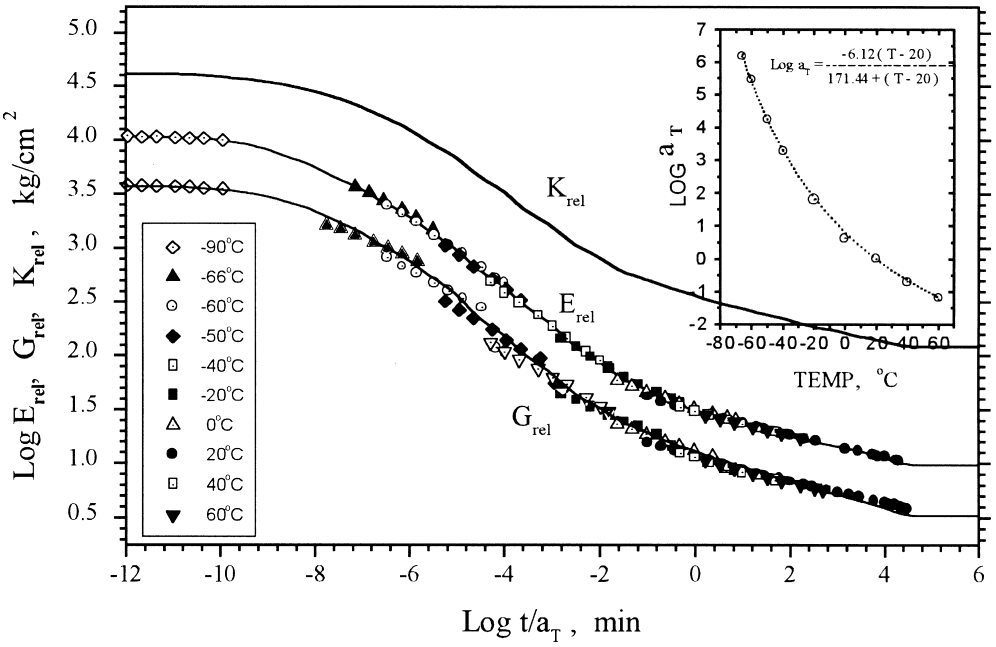

Fig. 5. Master relaxation modulus and shift factor.

assumed to be in simple shear. Since the glass transition temperature of HTPB propellant used is -80°C, the relaxation moduli at -90°C can be taken as glassy modulus. The master uniaxial/shear relaxation curves are obtained by horizontal shift only in time scale and well fitted with Prony series representation, eqns (33) and (34), as shown in Fig. 5. The shift factor a_T is also smoothly fitted with WLF eqn (35).

$$E^1_{\mathrm{rel}} = E_\infty + \sum_{i=1}^{16} E_i \mathrm{e}^{-\xi/\tau_i} \tag{33}$$

where

$$\xi = \int_0^t \frac{\mathrm{d}\tau}{a_{\mathrm{T}}(T(\tau))} \tag{34}$$

$$\mathrm{Log}\, a_{\mathrm{T}} = \frac{-6.12(T-20)}{171.44+(T-20)} \tag{35}$$

Therefore, thermorheologically simple behavior could be assumed. The shear relaxation modulus is close to the theoretical value, one-third of uniaxial modulus is magnitude. Thus, one can conclude that the solid propellant is nearly incompressible in small strain range. Also, the bulk modulus at small strain range is obtained by pocker chip test. The pocker chip test is conducted at strain rate 50% min^{-1} and in the temperature range of $-90 \sim 60^{\circ}$C. From the relation between the apparent

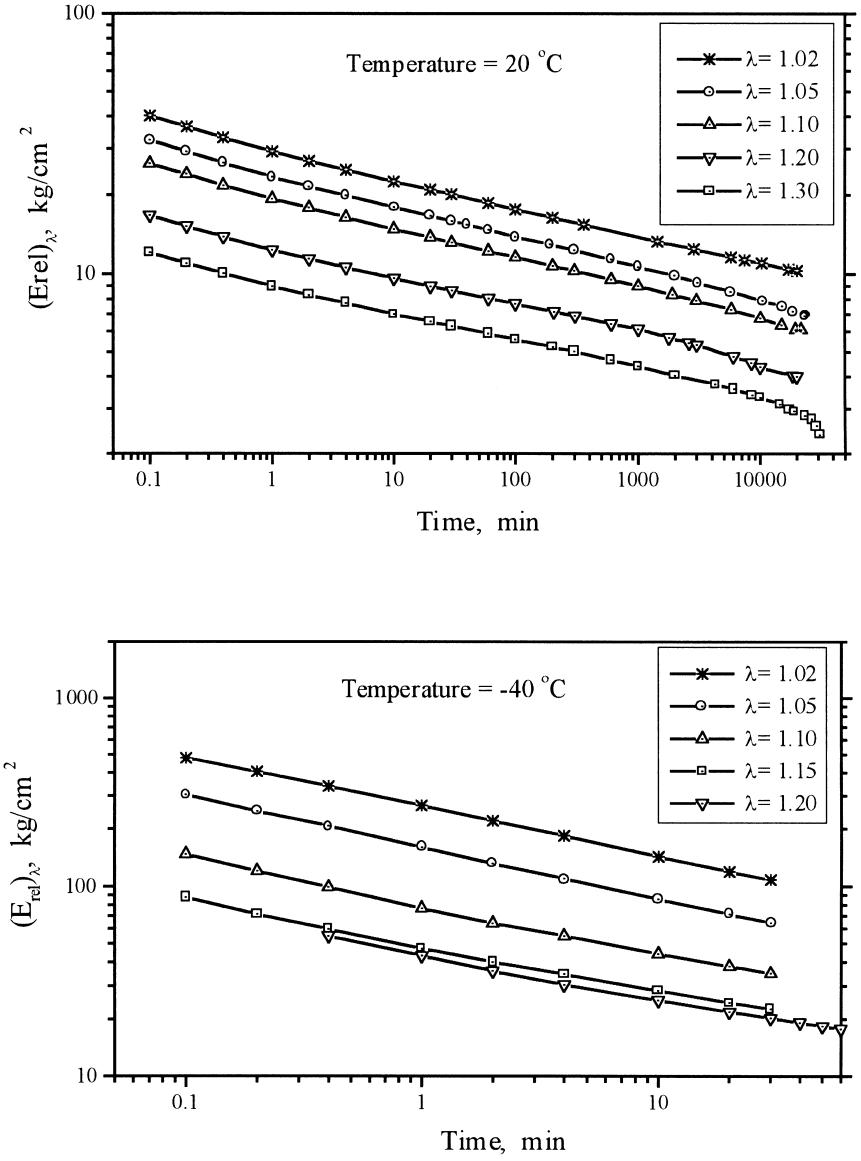

Fig. 6. Examples of uniaxial relaxation moduli at finite strains.

modulus of pocker chip specimen and the uniaxial modulus, the bulk relaxation modulus could be obtained (Schapery, 1988).

The uniaxial relaxation moduli at $\lambda = 1.05 \sim 1.30$, and $T = -40 \sim 60^{\circ}\mathrm{C}$ are measured for comparison with small strain modulus as shown in Fig. 6. The strain rate, $100 \sim 500\%\ \mathrm{min}^{-1}$ are applied to make the loading times uniform. The magnitudes of relaxation moduli at large stretches are decreased by damage due to dewetting. However, time characteristics are unchanged at all test

Table 1
Five different volume fractions of filler in relaxation test specimens

Filler type	Total vol. frac.				
	76.16% (Propellant)	58.36%	40.56%	22.94%	0% (Binder)
AP (200 μm)	35.60%	17.80%	0%	0%	0%
AP (70 μm)	17.62%	17.62%	17.62%	0%	0%
AP (6 μm)	21.67%	21.67%	21.67%	21.67%	0%
Al (5 μm)	1.27%	1.27%	1.27%	1.27%	0%

conditions compared with those of the linear relaxation modulus except long relaxation times beyond about one week. Therefore, the fourth constitutive assumption that time characteristics do not change by dewetting is verified at short times.

4.2. The effect of the filler volume fraction

In this study, the Farber–Farris equation is used to calculate propellant modulus for the variation of filler volume fraction. In order to confirm the applicability of eqn (5), small strain uniaxial and shear relaxation tests are conducted at 20°C. For this purpose, the five different propellant classes of varying filler volume fraction as in Table 1 are formulated and tested. The relaxation modulus is increased with the increase in the filler volume fraction. The predicted values from the current model and the experimental values of uniaxial relaxation modulus are shown in Fig. 7 at the relaxation time, 60 min for example. In Fig. 7, the relaxation modulus is shown to rapidly increase with the increase of the filler volume fraction and some difference between the predicted and measured values is observed. However, this discrepancy may be explained by the fact that the shape of AP particles used in the test is ellipsoidal while that of the theoretical model is spherical. The effect can be compensated by the relative volume fraction concept (Phillips, 1992), i.e. the shape effect of the filler can be accounted for by multiplying some constant to the volume fraction. This constant is obtained by matching the measured relaxation modulus values. The obtained constants with relaxation times are shown in Fig. 8. Its variation with the relaxation times is very small and thus its average value, 1.07157, could be used. The measured relaxation modulus can be well predicted by the effective value of the filler volume fraction, $c_{\text{eff}} = 1.07157 \times c$, as shown in Fig. 7.

4.3. The constant rate test

For the calculation of the decreased modulus, in eqn (5), the particle size distribution, volume fraction of the particles, matrix/filler modulus and the void properties are required. In the case of complete debonding the void's modulus can be counted as zero. However, this cannot happen in reality and the vacuoles may not truly be voids. The reasons are as follows:

For the solid propellant in which bonding agents are added to improve adhesion, complete

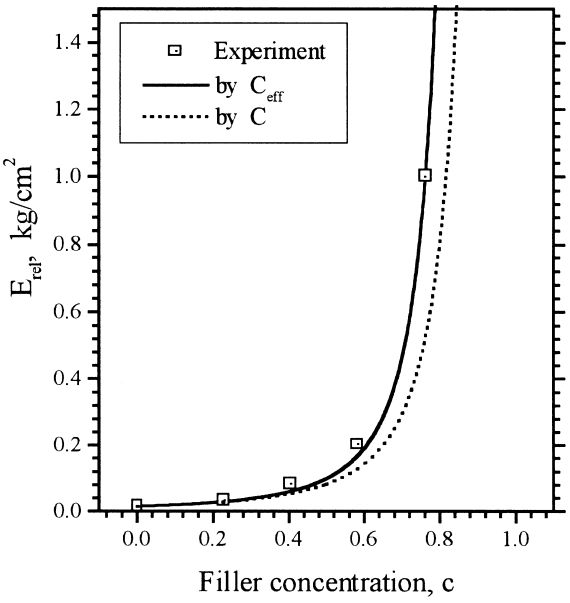

Fig. 7. Calculated relaxation modulus by c_{eff}.

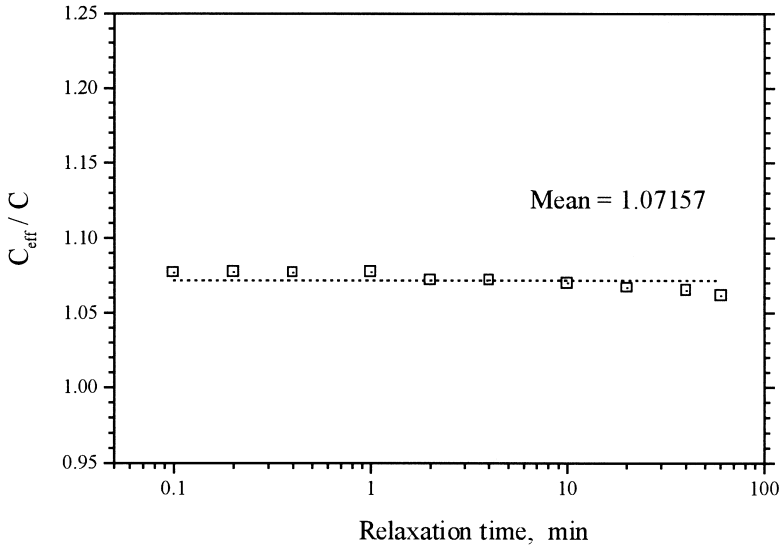

Fig. 8. Effective volume fraction vs relaxation time.

separation does not occur during the debonding process. Partial debonding of the particles and some degree of contact between the particle and the matrix still exists. Besides, even cohesive failure could occur (Gent and Park, 1984). In cohesive failure, vacuoles open around the particles

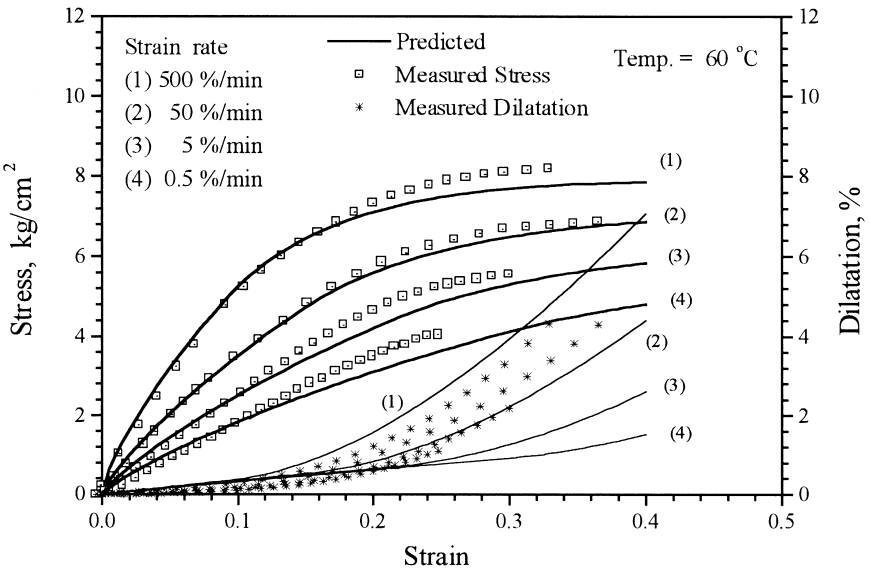

Fig. 9. Constant strain rate test at 60°C.

and some portion of matrix is still bonded to the particle surface. Also, the particle shape is not an exact sphere, which increases the possibility of partial debonding. Moreover, the effect of the existence of particle persists in the form of Poisson's effect in the lateral direction of applied strain. Thus the vacuoles are not complete voids and their moduli cannot be taken as zero in general.

Because the void's effective modulus cannot be determined by experiments, these values are determined by matching the observed constant rate stress–strain curves. From these calibrations, the void's shear modulus is deduced to be 1.5 times that of the propellant and the void's bulk modulus 1% that of the propellant.

The comparisons of the predicted and observed uniaxial stress–strain behaviors are shown in Figs 9–11 for the temperatures 60, 20 and -40°C and strain rates 0.5–500% min^{-1}. In general, the predicted stress responses are in good agreement with the measured ones. The use of non-zero void properties has the effect of lessening the degree of softening that is the realistic stress–strain behavior of the propellant. The calculated dilatations are distributed somewhat lower than the measured values. However, their trends are shown to be consistent.

4.4. The complex loading test

The constitutive model developed is used to predict the response of the solid propellant for different types of loading.

4.4.1. Dual strain rate test

The uniaxial specimen is loaded at dual strain rates at 20°C. In the first dual strain rate test, the rate is changed from 50 to 5% min^{-1} at the strain 11%. In the second dual strain rate test, the rate

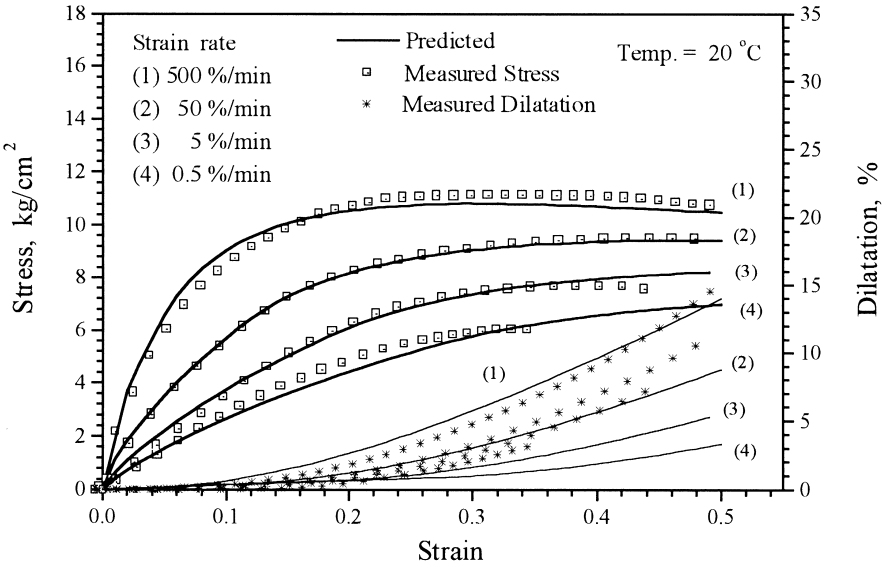

Fig. 10. Constant strain rate test at 20°C.

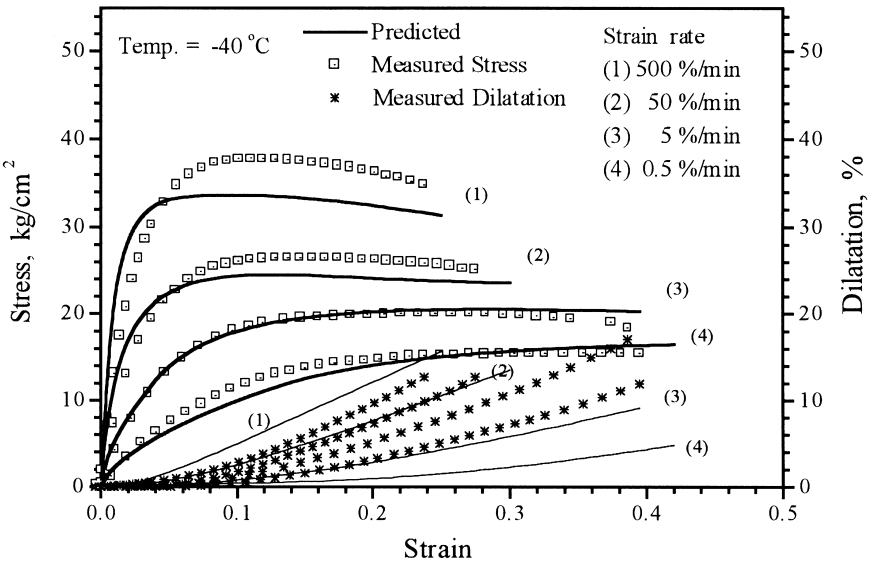

Fig. 11. Constant strain rate test at −40°C.

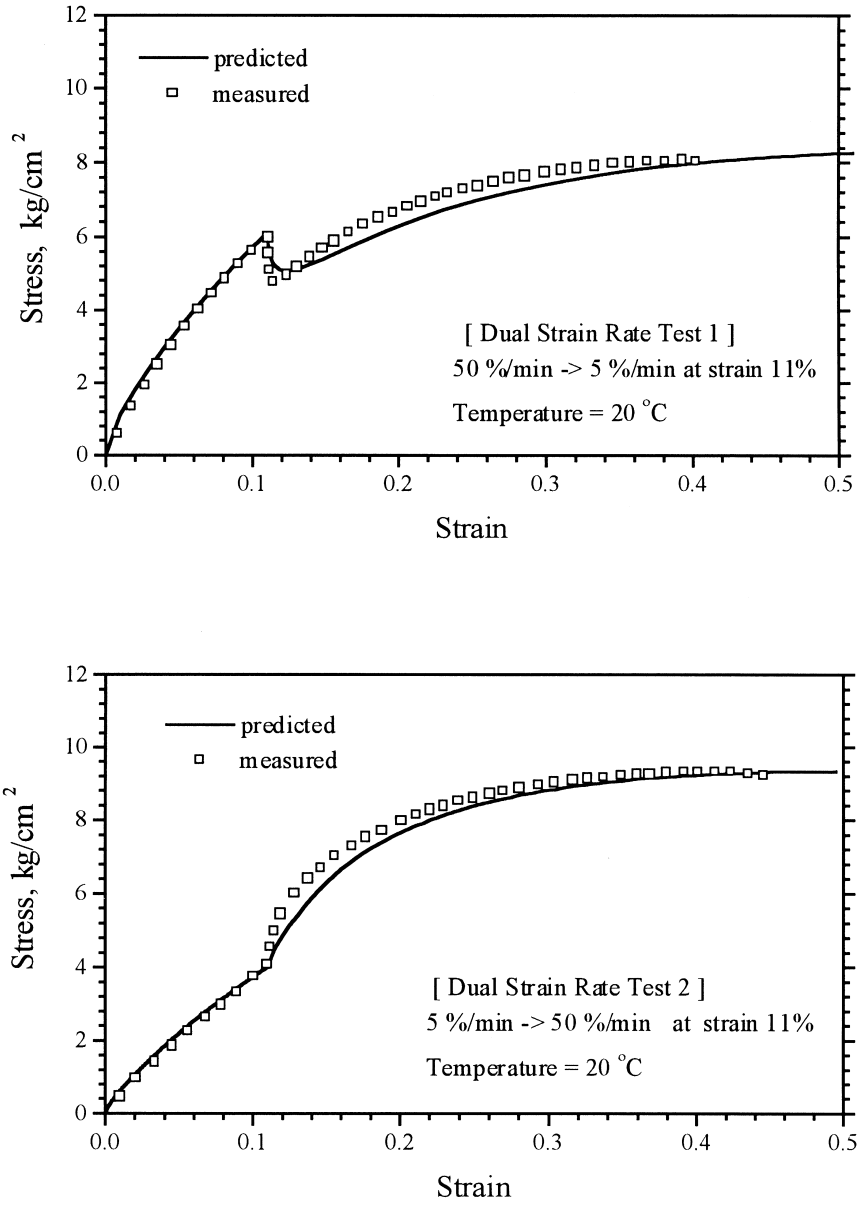

Fig. 12. Dual strain rate test at 20°C.

is changed from 5 to 50% min^{-1}. The comparison between the predicted and measured responses demonstrates the validity of the model, as shown in Fig. 12.

4.4.2. Cyclic loading test

Cyclic load is applied to the uniaxial sample at 20°C. The test is done with 10 cycles at strain levels of 0–20% and strain rate 50% min^{-1}. The damage functions f_u and f_r are determined from

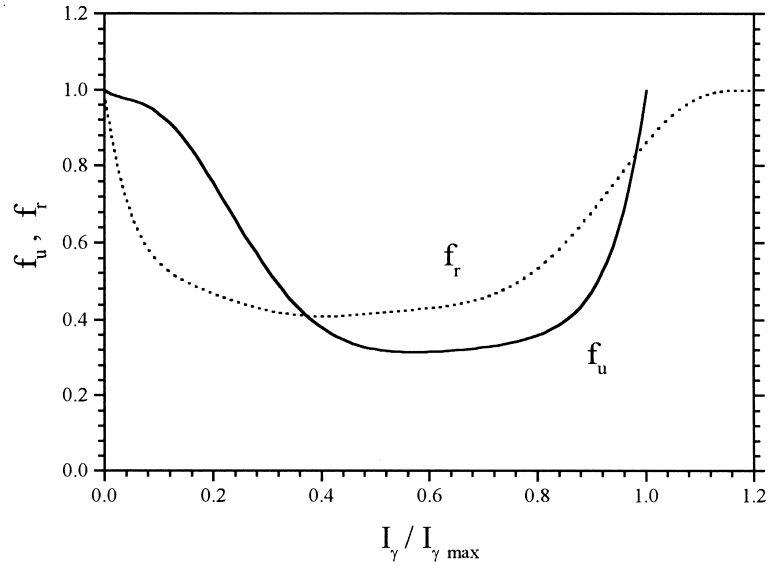

Fig. 13. Unloading and reloading functions, f_u, f_r.

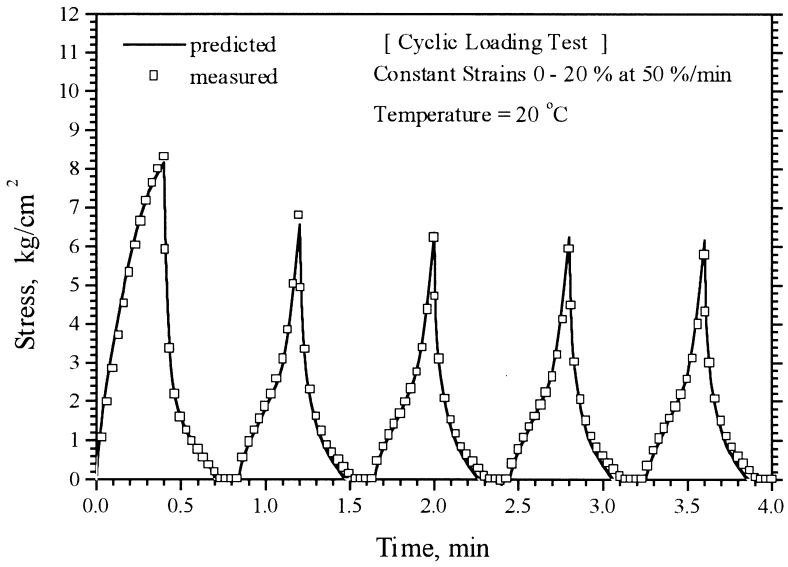

Fig. 14. Cycling test with const strain amplitude at 20°C.

the first loading-unloading cycle and are shown in Fig. 13. These functions are curve fitted with high-order polynomial functions and used in the calculation of damage functions. There is a good agreement between the predicted and measured stress, as shown in Fig. 14. Another cyclic test

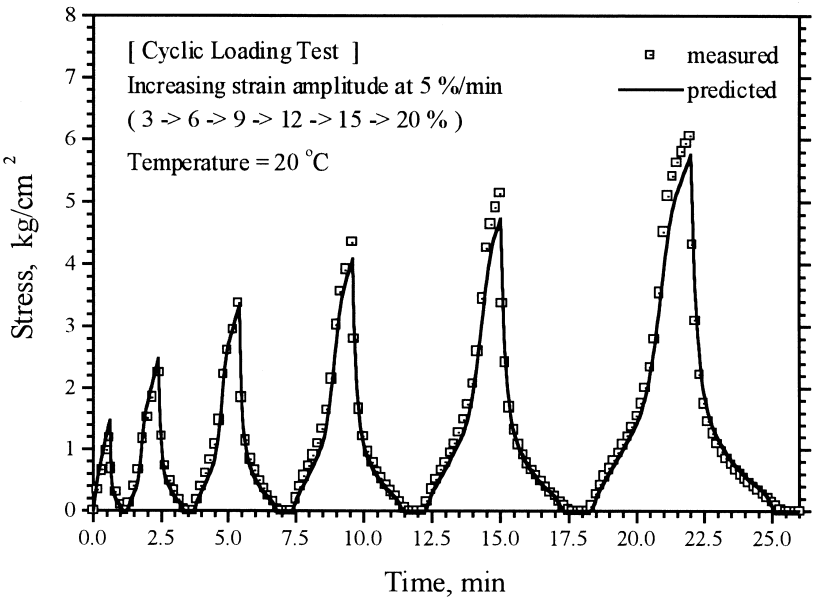

Fig. 15. Cycling test with increasing strain amplitude at 20°C.

with the increasing strain amplitude, 3, 6, 9, 12, 15 and 20% at 5% min^{-1}, 20°C is also conducted and the results are shown in Fig. 15.

4.4.3. Complex multiple load test

This test consists of subsequent loadings and unloadings at different strain levels at 50% min^{-1} and 20°C. The model predicts the stress response well as shown in Fig. 16.

4.4.4. Similitude test

The uniaxial specimen is loaded at strain rate 0.5% min^{-1} to the strain level 15% and then allowed to relax for 3 h. The relaxation is repeated for the strain of 5% and then the specimen is loaded to failure at 5% min^{-1}. While the relaxation response is somewhat underpredicted, the loading portions are well predicted as shown in Fig. 17. It can be observed that the dewetting does not greatly affect the relaxation nature of the propellant.

4.4.5. Straining and cooling test

The uniaxial specimen is loaded at 0.5% min^{-1}, while the temperature is lowered at a constant rate $-1°C\,min^{-1}$ from 60°C as shown in Fig. 18. The adhesion energies curve fitted with exponential function as in Fig. 4 are used for the varying temperature condition. The model underpredicts the magnitude of the stress.

5. Conclusion

The isotropic, viscoelastic constitutive model of composite solid propellant has been developed. The softening of the solid propellant is modeled by the modulus decrease which is caused by

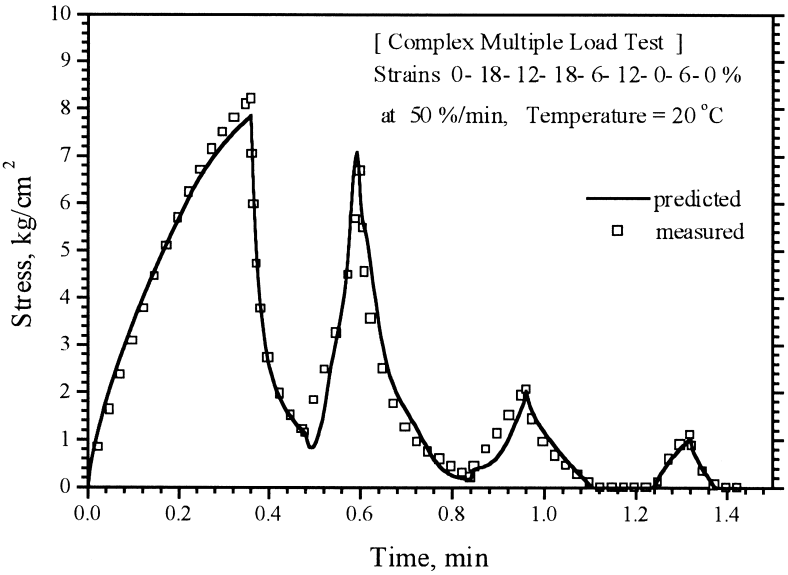

Fig. 16. Complex multiple load test at 20°C.

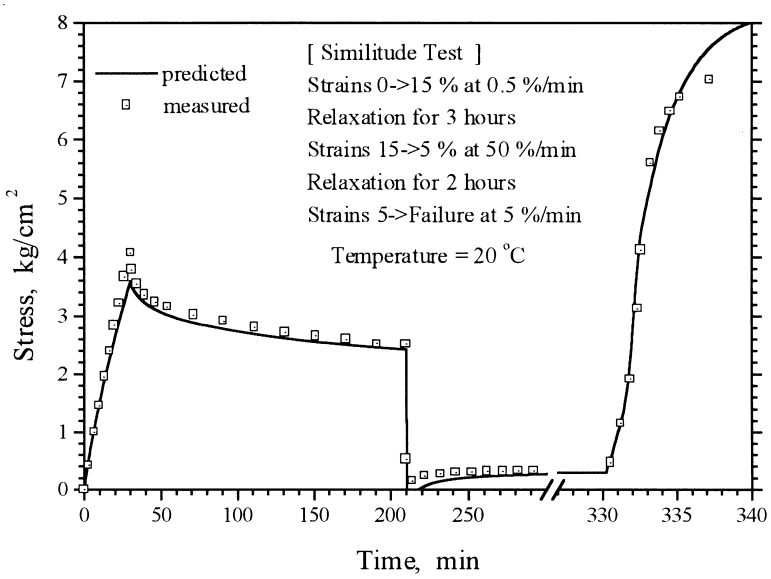

Fig. 17. Similitude test at 20°C.

dewetting. A viscoelastic dewetting criteria is developed and is used to predict the critical stress at which dewetting occurs. Also, the nonlinearities during unloading and reloading are treated by the functions of octahedral strain measure. The constitutive model has been tested for constant strain

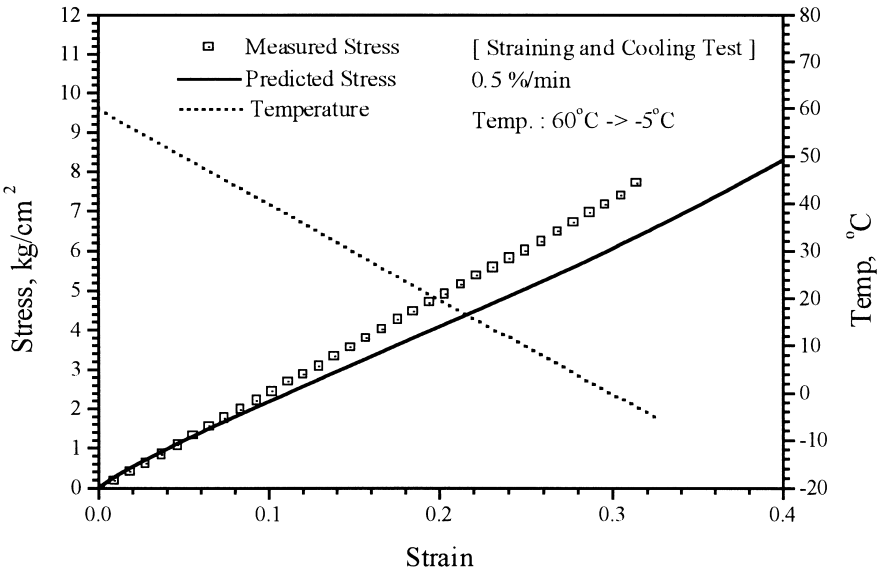

Fig. 18. Straining and cooling test.

rate conditions and the predictions have been compared with the experiments for several loading conditions. The results show that the model predicts the large range of the propellant behaviors with reasonable accuracies.

This model is relatively simple compared to other models which require many complicated nonlinear functions. Also, the present model can be used to predict composite solid propellants of different compositions since the model reflects the effects of the properties of the individual constituent in them.

References

ABAQUS Theory Manual, 1995. Viscoelasticity. Ver. 5.5., Hibbit, Karlsson and Sorensen, Inc., 4.7.1-1–4.

ASTM Standards No. D903-93, 1993. Standard test method for peel or stripping strength of adhesive bonds.

Farris, R.J., Schapery, R.A., 1973. Development of a solid rocket propellant nonlinear viscoelastic constitutive theory. AFRPL-TR-73-50.

Farber, J.N., Farris, R.J., 1987. Model for prediction of the elastic response of reinforced materials over wide ranges of concentration. J. Appl. Polym. Sic. 34, 2093–2104.

Gent, A.N., Park, B.K., 1984. Failure processes in elastomers at or near a rigid spherical inclusion. J. Mat. Sci. 19, 1947–1956.

Kugler, H.P., Stager, R.G., Steimle, C., 1990. Direct measurement of Poisson's ratio in elastomers. Rubber Chemistry and Technology 63, 473–487.

Özüpek, S., Becker, E.B., 1996. Constitutive equations for solid propellants. J. Engng Mat. Tech. 119, 125–132.

Phillips, M.G., 1992. Simple geometrical models for Young's modulus of fibrous and particulate composites. Composites Science and Technology 43, 95–100.

Ravichandran, G., Liu, C.T., 1995. Modeling constitutive behavior of particulate composites undergoing damage. Int. J. Solids Structures 32, 979–990.

Schapery, R.A., 1986. A micromechanical model for non-linear viscoelastic behavior of particulate-reinforced rubber with distributed damage. Engng. Frac. Mech. 25, 845–867.

Schapery, R.A., 1988. Solid Propellant Mechanical Behavior Manual, CPIA Pub. 21, 4.5.5-1–6.

Simo, J.C., 1987. On a fully three-dimensional finite strain viscoelastic damage model: formulation and computational aspects. Computer Methods in Appl. Mech. and Eng. 60, 153–173.

Swanson, S.R., Christensen, L.W., 1983. A constitutive formulation for high elongation propellant. J. Spacecraft 20, 559–566.

Vratsanos, L.A., Farris, R.J., 1993. A predictive model for the mechanical behavior of particulate composites. Part 1: Model derivation, Part 2: Comparison of model predictions to literature data. Polymer Eng. and Sci. 33, 1458–1474.